

Using Variational and PDE Methods for the Existence of Origami Models with Given Boundary Conditions

S.L. Keeling and R. Geretschläger

Abstract: *A tool based upon PDEs is developed to investigate the existence of an Origami model satisfying given boundary conditions. A mapping giving an Origami model is characterized by the condition of local rigidity, corresponding to a first-order system of nonlinear PDEs, which is solved subject to the prescribed boundary conditions. The variational approach is to minimize the equation residual plus vanishing regularization. The resulting optimality condition is solved by a steepest descent evolution equation. The discretization employs finite elements on unstructured grids conforming to the irregularity of a solution emerging near a fold. Existence of minimizers is proved together with the convergence of minimizers with vanishing regularization to an Origami model, provided one exists with the given boundary conditions.*

1 Introduction

The purpose of this work is to develop a tool based upon partial differential equations (PDEs) for investigating the existence of an Origami model satisfying given boundary conditions. For instance, on the left in Fig. 9 below, prescribed boundary conditions are emphasized as red curves, and the computed surface satisfying these boundary conditions indicates the existence of an associated Origami model.

To establish notation in the present context, let a flat paper be parameterized by points $\mathbf{x} = (x, y) \in \Omega = [0, 1]^2 \subset \mathbb{R}^2$. Let the transformed paper be given by the image of a mapping $\mathbf{u} = (u, v, w) : \Omega \rightarrow \mathbb{R}^3$. Such a mapping is modeled to be *locally rigid* [Dacorogna et al. 10] in the sense that

$$\nabla \mathbf{u}(\mathbf{x})^\top \nabla \mathbf{u}(\mathbf{x}) = I, \quad \mathbf{x} \in \Omega \setminus \Gamma, \quad \nabla \mathbf{u}(\mathbf{x}) = \begin{bmatrix} u_x(x, y) & u_y(x, y) \\ v_x(x, y) & v_y(x, y) \\ w_x(x, y) & w_y(x, y) \end{bmatrix} \quad (1)$$

where Γ is a possibly non-empty set of curves in Ω on which the paper may be folded. Otherwise, a solution to (1) is smooth on $\Omega \setminus \Gamma$. It can be shown with (1) that $\mathbf{u}(\Omega)$ has Gaussian curvature zero, i.e., it is developable, but such a property is not sufficient to guarantee all properties considered natural for folded or curved paper. A locally rigid transformation preserves not only Gaussian curvature but also lengths, angles and areas, since it is a local isometry [Dacorogna et al. 10].

to the uniqueness of such a solution. To relax the regularity assumptions in the convergence theorem, future investigations are proposed based upon approaches in mathematical image processing for dealing with edge sets.

2 The Optimality Condition

The system (4) is a necessary optimality condition on a minimizer \mathbf{u} of J in (3), and (4) is actually used to compute a minimizer. The necessary optimality condition is derived here, and then an iterative procedure is presented for its solution.

For a prospective minimizer \mathbf{u} with a perturbation $\bar{\mathbf{u}}$, the directional derivative of J in (3) is given by

$$\begin{aligned} \partial_{\mathbf{u}}J(\mathbf{u}; \bar{\mathbf{u}}) = \lim_{h \rightarrow 0} D_h J(\mathbf{u} + h\bar{\mathbf{u}}) = 4 \int_{\Omega} \left[(\|\mathbf{u}_x\|^2 - 1)(\mathbf{u}_x^{\top} \bar{\mathbf{u}}_x) + (\|\mathbf{u}_y\|^2 - 1)(\mathbf{u}_y^{\top} \bar{\mathbf{u}}_y) \right. \\ \left. + (\mathbf{u}_x^{\top} \mathbf{u}_y)(\bar{\mathbf{u}}_x^{\top} \mathbf{u}_y + \mathbf{u}_x^{\top} \bar{\mathbf{u}}_y) + \varepsilon \nabla^2 \mathbf{u} : \nabla^2 \bar{\mathbf{u}} \right] d\mathbf{x} \end{aligned} \quad (5)$$

where the last term is understood as the sum of all products of the respective fourth-order partial derivatives of \mathbf{u} and $\bar{\mathbf{u}}$. A minimizing \mathbf{u} has the property that $\partial_{\mathbf{u}}J(\mathbf{u}; \bar{\mathbf{u}}) = 0$ must hold for all permissible perturbations $\bar{\mathbf{u}}$. Since \mathbf{u} must satisfy fixed boundary conditions (2), and a perturbation may not disturb these conditions on the boundary, the set of permissible perturbations consists of smooth functions $\bar{\mathbf{u}}$ which vanish on the boundary $\partial\Omega$. The properties of $\bar{\mathbf{u}}$ may be exploited by integrating (5) by parts and assuming sufficient regularity of \mathbf{u} to obtain,

$$\begin{aligned} \frac{1}{4} \partial_{\mathbf{u}}J(\mathbf{u}; \bar{\mathbf{u}}) = & \int_{\partial\Omega} \bar{\mathbf{u}}^{\top} [n_x(\|\mathbf{u}_x\|^2 - 1)\mathbf{u}_x + n_y(\|\mathbf{u}_y\|^2 - 1)\mathbf{u}_y] d\sigma(\mathbf{x}) \\ & - \int_{\Omega} \bar{\mathbf{u}}^{\top} [((\|\mathbf{u}_x\|^2 - 1)\mathbf{u}_x)_x + ((\|\mathbf{u}_y\|^2 - 1)\mathbf{u}_y)_y] d\mathbf{x} \\ & \int_{\partial\Omega} \bar{\mathbf{u}}^{\top} [n_x(\mathbf{u}_y \mathbf{u}_y^{\top})\mathbf{u}_x + n_y(\mathbf{u}_x \mathbf{u}_x^{\top})\mathbf{u}_y] d\sigma(\mathbf{x}) \\ & - \int_{\Omega} \bar{\mathbf{u}}^{\top} \left[\left((\mathbf{u}_y^{\top} \mathbf{u}_x) \mathbf{u}_y \right)_x + \left((\mathbf{u}_x^{\top} \mathbf{u}_y) \mathbf{u}_x \right)_y \right] d\mathbf{x} \\ & \int_{\partial\Omega} \varepsilon \nabla \bar{\mathbf{u}}^{\top} \partial_n \nabla \mathbf{u} d\sigma(\mathbf{x}) - \int_{\partial\Omega} \varepsilon \bar{\mathbf{u}}^{\top} \partial_n \Delta \mathbf{u} d\sigma(\mathbf{x}) \\ & + \int_{\Omega} \varepsilon \bar{\mathbf{u}} \Delta^2 \mathbf{u} d\mathbf{x}. \end{aligned} \quad (6)$$

Since $\bar{\mathbf{u}} = 0$ holds on $\partial\Omega$, the boundary integrals $\int_{\partial\Omega} \bar{\mathbf{u}}^{\top} [\dots] d\sigma(\mathbf{x})$ in (6) vanish. Then $\bar{\mathbf{u}}$ may be chosen strategically so that all integrals in (6) are negligible except $\int_{\partial\Omega} \nabla \bar{\mathbf{u}}^{\top} [\varepsilon \partial_n \nabla \mathbf{u}] d\sigma(\mathbf{x})$. In this boundary integral $\partial_n \nabla \mathbf{u}$ is constrained to be pointwise zero by choosing $\bar{\mathbf{u}}$ further so that $\nabla \bar{\mathbf{u}}$ is concentrated at an arbitrary point on $\partial\Omega$. Thus, the boundary condition $\partial_n \nabla \mathbf{u} = 0$ on $\partial\Omega$ is obtained. Then only integrals over Ω remain in (6), and $\bar{\mathbf{u}}$ may be chosen strategically to be concentrated at an arbitrary point in Ω . Consequently, the sum of the respective integrands is constrained to be pointwise zero in Ω . As a result, the optimality condition for a minimizing \mathbf{u} is given by (4).

Since the left side of the differential equation in (4) can be viewed as a functional representation of the negative gradient of J in (3), a steepest descent approach to solving (4) is given by

$$\begin{cases} [(\|\mathbf{u}_x\|^2 - 1)\mathbf{u}_x]_x + [(\|\mathbf{u}_y\|^2 - 1)\mathbf{u}_y]_y + [((\mathbf{u}_y^\top \mathbf{u}_x)\mathbf{u}_y)_x + ((\mathbf{u}_x^\top \mathbf{u}_y)\mathbf{u}_x)_y] - \varepsilon \Delta^2 \mathbf{u} \\ \quad = \mathbf{u}_t, \quad \text{in } \Omega \times (0, \infty) \\ \mathbf{u} = \mathbf{e}, \quad \partial_n \nabla \mathbf{u} = 0 \quad \text{on } \partial\Omega \times [0, \infty) \quad \text{and} \quad \mathbf{u} = \mathbf{u}_0 \quad \text{in } \Omega \times \{0\}. \end{cases} \quad (7)$$

Here the variable t in $\mathbf{u}(\mathbf{x}, t)$ corresponds to *pseudo* time, used only as a temporal parameter indexing the course of the steepest descent evolution.

The qualitative properties of (7) can be gleaned by considering the model equation,

$$\begin{cases} [(u_x^2 - 1)u_x]_x - \varepsilon u_{xxxx} = u_t, & (x, t) \in (0, 1) \times (0, \infty) \\ u(0, t) = 0, \quad u(1, t) = 1, \quad u_{xx}(0, t) = u_{xx}(1, t) = 0, & t \in [0, \infty) \\ u(x, 0) = u_0(x), & x \in (0, 1) \end{cases}$$

corresponding to the case that $v = w = 0$ and $u = u(x, t)$. The steady state solution is $u_\infty(x) = x$, so the difference $\tilde{u} = u - u_\infty$ satisfies the boundary conditions $\tilde{u}(0, t) = \tilde{u}(1, t) = 0$ and $\tilde{u}_{xx}(0, t) = \tilde{u}_{xx}(1, t) = 0$. Now suppose that ε is sufficiently nontrivial that the fourth-order term dominates the evolution. Then the evolution equation $u_t = -\varepsilon u_{xxxx}$ is dissipative in the following sense. After integrating by parts and using the boundary conditions for the difference \tilde{u} , it follows that

$$\frac{1}{2} \partial_t \int_0^1 \tilde{u}^2 dx = \int_0^1 \tilde{u} \tilde{u}_t dx = \int_0^1 -\varepsilon \tilde{u}_{xxxx} \tilde{u} dx = \dots = -\varepsilon \int_0^1 \tilde{u}_{xx}^2 dx < 0$$

i.e., the integrated difference $\int_0^1 \tilde{u}^2(x, t) dx$ is decreasing. On the other hand, suppose that ε is small enough for the fourth-order term to be negligible, and assume that $u_x^2 - 1 \approx \kappa > 0$. Then the evolution equation $u_t = [\kappa u_x]_x$ is also dissipative, i.e., after integrating by parts and using the boundary conditions for \tilde{u} ,

$$\frac{1}{2} \partial_t \int_0^1 \tilde{u}^2 dx = \int_0^1 \tilde{u} \tilde{u}_t dx = \int_0^1 \tilde{u} [\kappa \tilde{u}_x]_x dx = \dots = -\int_0^1 \kappa \tilde{u}_x^2 dx < 0.$$

Yet the same calculations show that for $\kappa < 0$ the evolution equation is accretive, i.e., the integrated difference $\int_0^1 \tilde{u}^2(x, t) dx$ is increasing. Thus the dissipative and accretive forces oppose each other. Provided the unstable accretive forces are sufficiently balanced by the stable dissipative forces, a non-trivial steady state is achieved. For $\varepsilon > 0$, the dissipative forces in (7) are always sufficient to establish a stable evolution to the desired steady state which solves (4). Yet, for ever decreasing ε , the convergence of these ε -dependent steady states requires the existence of an Origami model associated with the prescribed boundary conditions.

The necessary optimality condition (4) and the associated steepest descent evolution (7) are said to be posed in *strong* form because they presuppose sufficient smoothness in the solution so that all the terms appearing in the respective systems

are well defined. The finite difference method amounts to approximating derivatives with difference quotients, and the method is well suited to a direct discretization of the strong form of a PDE. As indicated in Section 1, finite differences are adequate to solve (4) or (7), provided there are no folds or that a fold conforms to a line in the grid used to discretize the spatial domain Ω . For more general cases, it is necessary to employ a discretization method which can accommodate general folds and a lack of regularity in the solution at a fold. The first step is to obtain a *weak* form of the optimality condition (4) in which less smoothness is required of \mathbf{u} [Showalter 77]. For this, it is required directly that the directional derivatives in (5) vanish for all permissible perturbations $\bar{\mathbf{u}}$,

$$\frac{1}{4} \partial_{\mathbf{u}} J(\mathbf{u}; \bar{\mathbf{u}}) = a(\mathbf{u}, \mathbf{u}, \bar{\mathbf{u}}) = 0, \quad \forall \bar{\mathbf{u}} \text{ smooth in } \Omega \text{ and } \bar{\mathbf{u}} = 0 \text{ on } \partial\Omega \quad (8)$$

subject to the boundary conditions (2) where explicitly

$$a(\mathbf{u}, \hat{\mathbf{u}}, \check{\mathbf{u}}) = \int_{\Omega} \left[(\|\mathbf{u}_x\|^2 - 1)(\hat{\mathbf{u}}_x^{\top} \check{\mathbf{u}}_x) + (\|\mathbf{u}_y\|^2 - 1)(\hat{\mathbf{u}}_y^{\top} \check{\mathbf{u}}_y) + (\mathbf{u}_x^{\top} \mathbf{u}_y)(\hat{\mathbf{u}}_x^{\top} \check{\mathbf{u}}_y + \check{\mathbf{u}}_x^{\top} \hat{\mathbf{u}}_y) + \varepsilon \nabla^2 \check{\mathbf{u}} : \nabla^2 \hat{\mathbf{u}} \right] d\mathbf{x}. \quad (9)$$

Then with

$$b(\mathbf{u}, \bar{\mathbf{u}}) = \int_{\Omega} \bar{\mathbf{u}}^{\top} \mathbf{u} d\mathbf{x} \quad (10)$$

the corresponding weak form of the steepest descent evolution (7) is given by

$$b(\mathbf{u}_t(t), \bar{\mathbf{u}}) = -a(\mathbf{u}(t), \mathbf{u}(t), \bar{\mathbf{u}}), \quad \forall t \in [0, T], \quad \forall \bar{\mathbf{u}} \text{ smooth in } \Omega \text{ and } \bar{\mathbf{u}} = 0 \text{ on } \partial\Omega \quad (11)$$

subject to the boundary conditions (2), i.e., $u(\mathbf{x}, t) = \mathbf{e}(\mathbf{x})$, $\mathbf{x} \in \partial\Omega$, $t \geq 0$. The essence of the finite element method detailed in Section 3 is to approximate the solution \mathbf{u} and the permissible perturbations $\bar{\mathbf{u}}$ in (8) and (11) with the span of simple functions which can be computed easily and which can approximate a desired solution with a desired accuracy.

3 Numerical Discretization with Finite Elements

To define a suitable basis of functions for approximating a solution to (8) or (11), the spatial domain Ω is first triangulated. Let Ω be discretized into Delaunay triangles $\{T_e\}_{e=1}^E$ with vertices taken from nodes $\{\mathbf{x}_n = (x_n, y_n)\}_{n=1}^N \subset \Omega$ where, by definition of a Delaunay triangle, no node \mathbf{x}_n is inside the circumcircle of any triangle T_e . It is intended that nodes not only be scattered throughout the interior of Ω and on $\partial\Omega$ but also that they be strategically located on and near a paper fold to accommodate the associated lack of regularity in the solution to (7). Let the temporal domain be discretized with nodes, $t^k = k\Delta t$, $k = 0, \dots, N_t$, $\Delta t = T/N_t$, where T is the maximal time to which the system is solved.

Given the above triangulation of Ω , it suffices here to define the desired approximation basis as the span of the piecewise linear functions $\{\phi_n\}_{n=1}^N$ where each ϕ_n is (a) a linear polynomial on each element T_e , (b) equal to 1 on the node \mathbf{x}_n and 0

on every other node \mathbf{x}_m , $m \neq n$, and (c) globally continuous on Ω . In other words, the plot of the function ϕ_n appears like a *tent* with its peak at \mathbf{x}_n , fastened to the ground at all neighboring nodes and remaining on the ground outside the elements T_e with vertex \mathbf{x}_n . Given these tent functions, denote the approximation space by $S_N(\Omega) = \text{span}\{\phi_n\}_{n=1}^N$ and denote by $S_{N,0}(\Omega)$ the subspace of those functions in $S_N(\Omega)$ which vanish on the boundary $\partial\Omega$.

To approximate a solution $\mathbf{u} = \mathbf{u}(\mathbf{x})$ to the weak form (8) of the optimality system, an element $\mathbf{u}_N = \mathbf{u}_N(\mathbf{x})$ of the Cartesian product $S_N(\Omega)^3 = S_n(\Omega) \times S_n(\Omega) \times S_n(\Omega)$ is used,

$$\mathbf{u}_N(\mathbf{x}) = \sum_{n=1}^N \mathbf{u}_n \phi_n(\mathbf{x}), \quad \mathbf{u}_N(\mathbf{x}_n) \approx \mathbf{u}(\mathbf{x}_n).$$

To approximate a solution $\mathbf{u} = \mathbf{u}(\mathbf{x}, t)$ to the weak form (11) of the steepest descent evolution, the terms above depend also upon k , i.e.,

$$\mathbf{u}_N^k(\mathbf{x}) = \sum_{n=1}^N \mathbf{u}_n^k \phi_n(\mathbf{x}), \quad \mathbf{u}_N^k(\mathbf{x}_n) \approx \mathbf{u}(\mathbf{x}_n, t^k), \quad k = 0, \dots, N_t.$$

An approximate solution to the weak optimality system (8) is obtained through a finite element approach by computing a function $\mathbf{u}_N \in S_N(\Omega)^3$ satisfying

$$a(\mathbf{u}_N, \mathbf{u}_N, \Phi) = 0, \quad \forall \Phi \in S_{N,0}(\Omega)^3 \quad (12)$$

subject to the discrete boundary conditions corresponding to (2),

$$\mathbf{u}_N(\mathbf{x}_n) = \mathbf{e}(\mathbf{x}_n), \quad \mathbf{x}_n \in \partial\Omega. \quad (13)$$

An approximate solution to the weak form (11) of the steepest descent evolution is obtained through a finite element approach by computing functions $\{\mathbf{u}_N^k\}_{k=0}^{N_t} \subset S_N(\Omega)^3$ satisfying

$$b([\mathbf{u}_N^{k+1} - \mathbf{u}_N^k]/\Delta t, \Phi) = - \left[a_1(\mathbf{u}_N^k, \mathbf{u}_N^{k+1}, \Phi) + a_2(\mathbf{u}_N^k, \Phi) + a_3(\mathbf{u}_N^k, \mathbf{u}_N^k, \Phi) + a_4(\mathbf{u}_N^{k+1}, \Phi) \right] \quad (14)$$

$$\forall \Phi \in S_{N,0}(\Omega)^3, \quad k = 0, \dots, N_t - 1$$

subject to the discrete boundary conditions corresponding to (2),

$$\mathbf{u}_N^k(\mathbf{x}_n) = \mathbf{e}(\mathbf{x}_n), \quad \mathbf{x}_n \in \partial\Omega, \quad k = 0, \dots, N_t \quad (15)$$

where b is given in (10) and a in (9) has been decomposed according to

$$\begin{aligned} a(\mathbf{u}, \hat{\mathbf{u}}, \check{\mathbf{u}}) &= a_1(\mathbf{u}, \hat{\mathbf{u}}, \check{\mathbf{u}}) + a_2(\hat{\mathbf{u}}, \check{\mathbf{u}}) + a_3(\mathbf{u}, \hat{\mathbf{u}}, \check{\mathbf{u}}) + a_4(\hat{\mathbf{u}}, \check{\mathbf{u}}) \\ a_1(\mathbf{u}, \hat{\mathbf{u}}, \check{\mathbf{u}}) &= \int_{\Omega} \left[\|\mathbf{u}_x\|^2 (\hat{\mathbf{u}}_x^\top \check{\mathbf{u}}_x) + \|\mathbf{u}_y\|^2 (\hat{\mathbf{u}}_y^\top \check{\mathbf{u}}_y) \right] d\mathbf{x} \\ a_2(\hat{\mathbf{u}}, \check{\mathbf{u}}) &= - \int_{\Omega} \left[(\hat{\mathbf{u}}_x^\top \check{\mathbf{u}}_x) + (\hat{\mathbf{u}}_y^\top \check{\mathbf{u}}_y) \right] d\mathbf{x} \\ a_3(\mathbf{u}, \hat{\mathbf{u}}, \check{\mathbf{u}}) &= \int_{\Omega} \left[(\mathbf{u}_x^\top \mathbf{u}_y) (\hat{\mathbf{u}}_x^\top \check{\mathbf{u}}_y + \check{\mathbf{u}}_x^\top \hat{\mathbf{u}}_y) \right] d\mathbf{x} \\ a_4(\hat{\mathbf{u}}, \check{\mathbf{u}}) &= \varepsilon \int_{\Omega} [\nabla(P\nabla\check{\mathbf{u}})] : [\nabla(P\nabla\hat{\mathbf{u}})] d\mathbf{x} \end{aligned}$$

where P in a_4 is a projection into $S_N(\Omega)^6$. If the right side in (14) were replaced by the form a from (9) evaluated purely at the state \mathbf{u}_N^k known at time t^k , then the new state \mathbf{u}_N^{k+1} would be explicitly defined in terms of the old state \mathbf{u}_N^k by (14). Such an explicit scheme would be easy and inexpensive to implement, but it is not sufficiently stable. On the other hand, if the right side in (14) were replaced by the form a evaluated purely at the state \mathbf{u}_N^{k+1} unknown at time t^{k+1} , then the new state \mathbf{u}_N^{k+1} would be only implicitly defined in terms of the old state \mathbf{u}_N^k by (14). Such an implicit scheme would be stable but unnecessarily complex and expensive to solve. The mixture of states \mathbf{u}_N^k and \mathbf{u}_N^{k+1} appearing in (14) provides a balance of stability and limited overhead. Furthermore, once all terms with \mathbf{u}_N^{k+1} are grouped together in a linear system $L(\mathbf{u}_N^k)\mathbf{u}_N^{k+1} = F(\mathbf{u}_N^k)$ with known $L(\mathbf{u}_N^k)$ and $F(\mathbf{u}_N^k)$ depending upon \mathbf{u}_N^k , the coefficient matrix emerging on the left side of this system of time stepping equations is symmetric and positive definite. This property ensures the solvability of the time stepping system and that the step from \mathbf{u}_N^k to \mathbf{u}_N^{k+1} is a descent direction for the minimization of J . A Newton method for solving (12) has also been implemented and found in the present context to be less efficient than the proposed time stepping especially with large time steps.

4 Computational Results

In this section examples are presented to demonstrate the results of the methods proposed above. All computations were performed with Matlab.* What are not shown in this section are examples in which boundary conditions (2) are imposed which are known to be unfriendly to an Origami model so that no solution to (1) exists satisfying these boundary conditions. In such cases, (4) is of course solvable for $\varepsilon > 0$, but the solutions do not converge as $\varepsilon \rightarrow 0$. In each of the following cases, an exact solution \mathbf{u}^* to (1) and (2) is known in advance, and the initial values \mathbf{u}_0 in (7) are determined by the following simple method of continuing the prescribed boundary conditions (2) smoothly into the interior of Ω ,

$$\begin{cases} \Delta \mathbf{u}_0 = 0 & \text{in } \Omega \\ \mathbf{u}_0 = \mathbf{e} & \text{on } \partial\Omega. \end{cases} \quad (16)$$

The initial values can of course be chosen closer to the known solution, but (16) is used to extend the boundary conditions into the interior of Ω as if no better estimate of the solution were available.

4.1 Example 1

As seen in Fig. 3 below, this example corresponds to a paper curved to have a parabolic profile. The prescribed boundary conditions are emphasized in red on the left in Fig. 3. An exact solution to (1) and (2) is given as follows. First, $u = u(x)$ is chosen to solve the initial value problem,

$$u'(x)^2 + [2\sigma u(x)[1 - 2u(x)]']^2 = 1, \quad x \in [0, 1], \quad u(0) = 0$$

*<http://www.mathworks.com>

and the scaling constant σ is chosen so that $u(1) = 1/2$. Then

$$v = v(x) = 2\sigma u(x)[1 - 2u(x)], \quad w = w(y) = y.$$

It can be seen as follows that there is no other solution to (1) which satisfies the same boundary conditions (2). The above solution can be described as an ensemble of straight vertical lines, each of length one and connecting the edges prescribed at the top and at the bottom. This is the only solution since any geodesic emanating vertically from the bottom edge to connect with the top edge would have length greater than the required value of one if it were not a straight line.

The triangulation of the unfolded paper is shown on the left in Fig. 1. Since there is no fold, there is no accumulation of nodes to accommodate such a fold. Fig. 2 shows the initial conditions for this example on the left, which are clearly

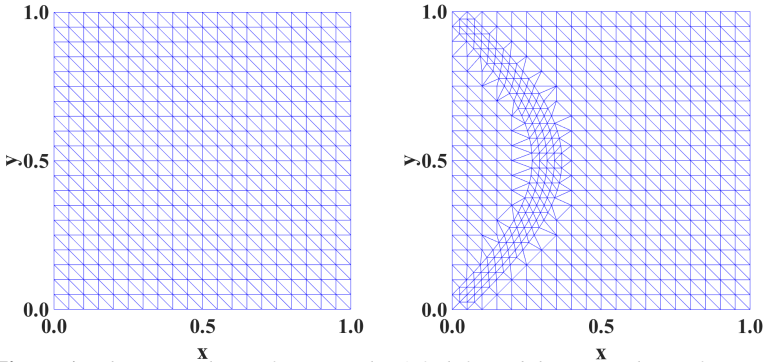


Figure 1: The triangulation for Examples 1-3 (left) and the triangulation for Example 4 (right).

smoothed due to the initial use of (16). The middle plot of Fig. 2 shows the distri-

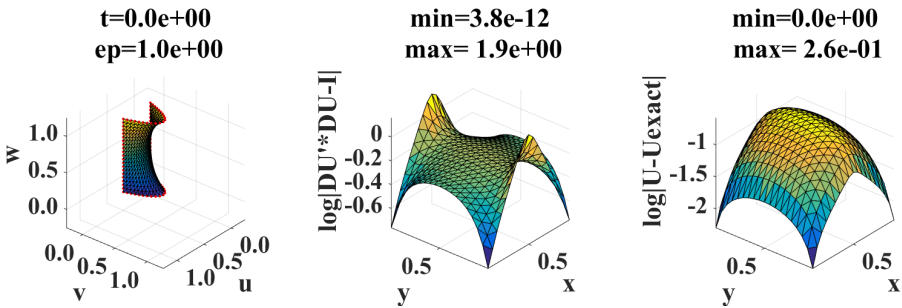


Figure 2: Initial shape (left), residuals (middle) and error (right) for Example 1.

bution of residual values for (1),

$$\log_{10} \|\nabla \mathbf{u}^\top \nabla \mathbf{u} - I\|_F \tag{17}$$

which depart significantly from zero since the paper is initially smoothed. In particular, these residual values are especially large near the middle of the parabolic profiles on the boundary, and they are relatively smaller in the corners of the smoothed paper where deformation is less. The plot on the right in Fig. 2 shows the pointwise departure of the computed solution \mathbf{u} from the known exact solution \mathbf{u}^* ,

$$\log_{10} \|\mathbf{u} - \mathbf{u}^*\| \tag{18}$$

and these values are also non-trivial, achieving a maximum in the center of the smoothed paper.

After convergence of the iteration (14), the result shown in Fig. 3 is obtained. The computed surface is shown on the left in Fig. 3, which can be seen to be quite

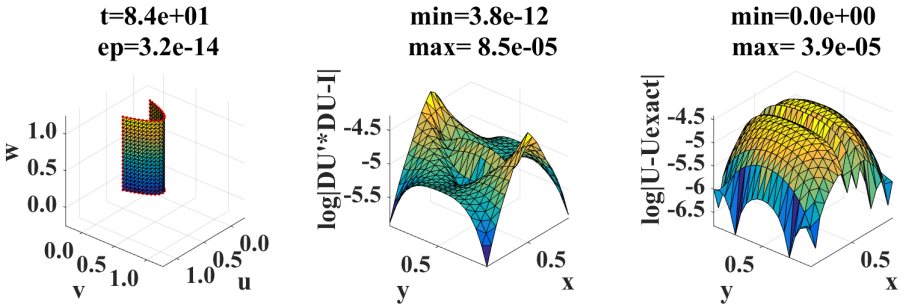


Figure 3: Final shape (left), residuals (middle) and error (right) for Example 1.

accurate based purely upon visual inspection. The middle plot in Fig. 3 shows the residual values (17), which are at most $8.5 \cdot 10^{-5}$. The right plot in Fig. 3 shows the error values (18), which are at most $3.9 \cdot 10^{-5}$.

4.2 Example 2

As seen in Fig. 5 below, this example corresponds to a paper folded once into two equal pieces and each side of the folded paper is either parallel or perpendicular to the fold. The prescribed boundary conditions are emphasized in red on the left in Fig. 5. An exact solution to (1) and (2) is given as follows:

$$u = u(x) = \frac{x}{2}, \quad v = v(x) = \frac{\sqrt{3}}{2} \begin{cases} x, & x < 1/2 \\ (1-x), & x \geq 1/2, \end{cases} \quad w = w(y) = y.$$

The fold is located at $x = 1/2$. The same argument as applied to Example 1 shows for this example that there is no other solution to (1) satisfying the same boundary conditions (2).

The triangulation of the unfolded paper is the same as that shown on the left in Fig. 1 for Example 1. In particular, no additional nodes have been introduced near the fold, which actually conforms to triangle edges along the line $x = 1/2$.

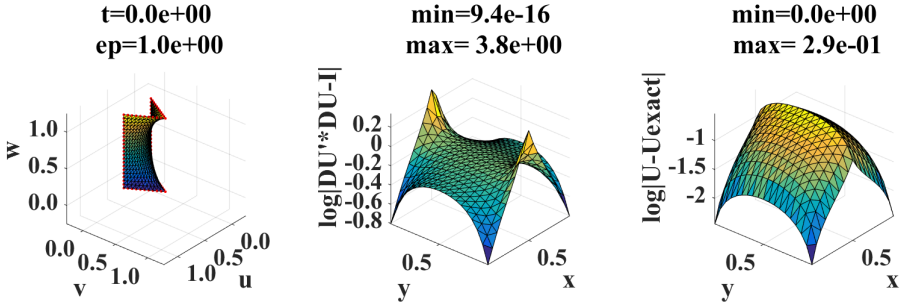


Figure 4: Initial shape (left), residuals (middle) and error (right) for Example 2.

Fig. 4 shows the initial conditions for this example on the left, which are clearly smoothed due to the initial use of (16). The middle plot in Fig. 4 shows the distribution of the residual values (17), which depart significantly from zero since the paper is initially smoothed. The plot on the right in Fig. 4 shows the error values (18), which are also non-trivial, achieving a maximum along the paper fold.

After convergence of the iteration (14), the result shown in Fig. 5 is obtained. The computed surface is shown on the left in Fig. 5, which can be seen to be quite

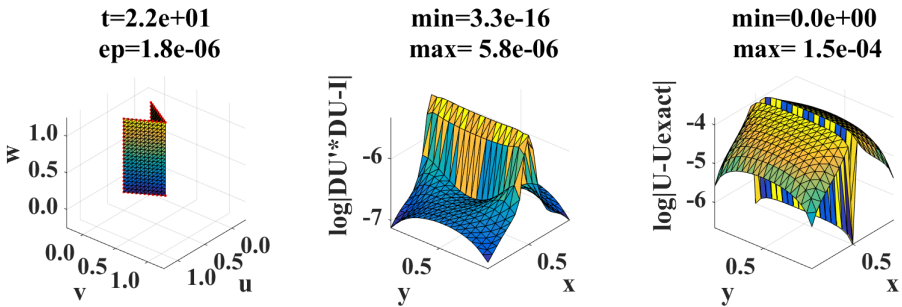


Figure 5: Final shape (left), residuals (middle) and error (right) for Example 2.

accurate based purely upon visual inspection. The middle plot in Fig. 5 shows the residual values (17), which are at most $5.8 \cdot 10^{-6}$, and such values are found along the fold. The right plot in Fig. 5 shows the error values (18), which are at most $1.5 \cdot 10^{-4}$, as observed adjacent to the paper fold.

4.3 Example 3

As seen in Fig. 7 below, this example corresponds to a paper folded diagonally once into two equal and triangular pieces, and the fold connects opposite corners of the paper. The prescribed boundary conditions are emphasized in red on the left

in Fig. 7. An exact solution $\mathbf{u} = (u, v, w)$ to (1) and (2) is given as follows:

$$\mathbf{u}(x, y) = \begin{pmatrix} x \\ y \\ 0 \end{pmatrix}, \quad y \leq 1 - x, \quad \mathbf{u}(x, y) = \begin{pmatrix} \frac{1}{2}(x + 1 - y) \\ \frac{1}{2}(y + 1 - x) \\ \frac{1}{\sqrt{2}}(x + y - 1) \end{pmatrix}, \quad y \geq 1 - x.$$

It can be seen as follows that there is no other solution to (1) which satisfies the same boundary conditions (2). Consider one of the triangles formed by the fold in the solution above. Points on opposite sides of and at an equal distance ℓ from the right angle in the triangle are separated by a distance $\sqrt{2}\ell$ in the paper. This is the only solution since any geodesic connecting such points would have length greater than the required value of $\sqrt{2}\ell$ if it were not a straight line.

The triangulation of the unfolded paper is the same as that on the left in Fig. 1 for Example 1. In particular, no additional nodes have been introduced near the fold, which actually conforms to triangle edges along the line $y = 1 - x$.

Fig. 6 shows the initial conditions for this example on the left, which are clearly smoothed due to the initial use of (16). The middle plot in Fig. 6 shows the distribu-

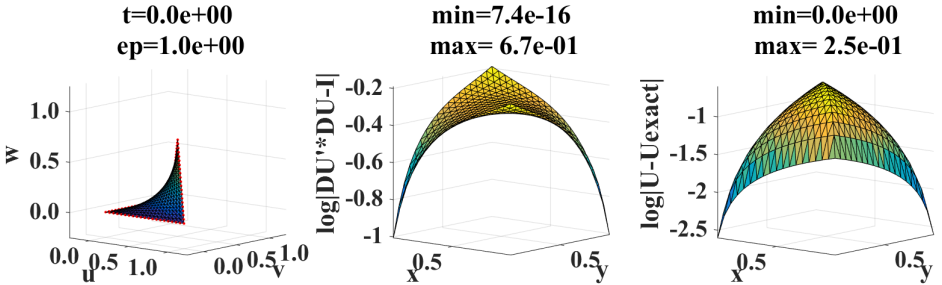


Figure 6: Initial shape (left), residuals (middle) and error (right) for Example 3.

tion of residual values (17), which depart significantly from zero since the paper is initially smoothed. In particular, these residual values are especially large near the smoothed fold and they are relatively smaller in the corners of the smoothed paper where deformation is less. The plot on the right in Fig. 6 shows the error values (18), and these values are also non-trivial, achieving a maximum in the smoothed fold of the paper.

After convergence of the iteration (14), the result shown in Fig. 7 is obtained. The computed surface is shown on the left in Fig. 7, which can be seen to be quite accurate based purely upon visual inspection. The middle plot in Fig. 7 shows the residual values (17), which are at most $9.8 \cdot 10^{-6}$ along the fold. The right plot in Fig. 7 shows the error values (18), which are at most $2.6 \cdot 10^{-4}$ adjacent to the fold.

4.4 Example 4

As seen in Fig. 9 below, this example corresponds to a paper folded in a curved fashion to create two adjoining circular cylinders. The prescribed boundary con-

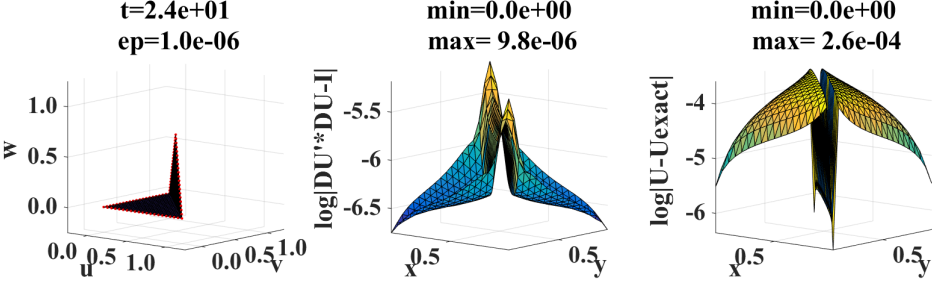


Figure 7: Final shape (left), residuals (middle) and error (right) for Example 3.

ditions are emphasized in red on the left in Fig. 9. The example is taken from [Geretschläger 09]. An exact solution to (1) and (2) is given as follows. First, $u(y)$ is chosen to solve the initial value problem,

$$u'(y)^2 + [\sigma \sqrt{u(y)[2/\pi - u(y)]}]^2 = 1, \quad y \in [0, 1], \quad u(0) = 0$$

and the scaling constant σ is chosen so that $u(1) = 2/\pi$ holds. Then for $\pi x \leq \sin(\pi y)$,

$$u = u(y), \quad v = v(x) = x, \quad w = w(y) = \sigma \sqrt{u(y)[2/\pi - u(y)]}$$

and for $\pi x \geq \sin(\pi y)$,

$$u = u(y), \quad v = v(y) = s \sqrt{u(y)[2/\pi - u(y)]}, \quad w = w(x) = x.$$

On the basis of computational results shown below, one concludes that there is no other solution to (1) satisfying the same boundary conditions (2), but no theoretical argument is presented here.

The triangulation of the paper is shown on the right in Fig. 1. Note that this triangulation is identical to that used in the previous examples except that for this example additional nodes are accumulated along and near the curved fold.

Fig. 8 shows the initial conditions for this example on the left, which are clearly smoothed due to the initial use of (16). The middle plot in Fig. 8 shows the distribution of residual values (17), which depart significantly from zero since the paper is initially smoothed. In particular, these residual values are especially large on the side of the paper nearest the curved fold, and they are relatively smaller in the corners of the paper farthest away from the fold where deformation is less. The plot on the right in Fig. 8 shows the error values (18), and these values are also non-trivial, achieving a maximum in the smoothed fold of the paper.

After convergence of the iteration (14), the result shown in Fig. 9 is obtained. The computed surface is shown on the left in Fig. 9, which can be seen to be quite accurate based purely upon visual inspection. The middle plot in Fig. 9 shows that

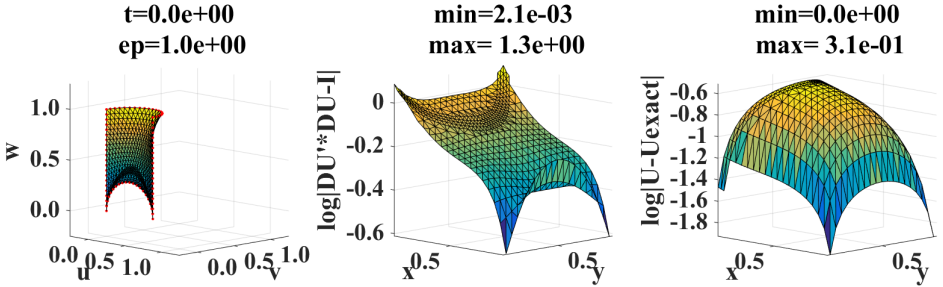


Figure 8: Initial shape (left), residuals (middle) and error (right) for Example 4.

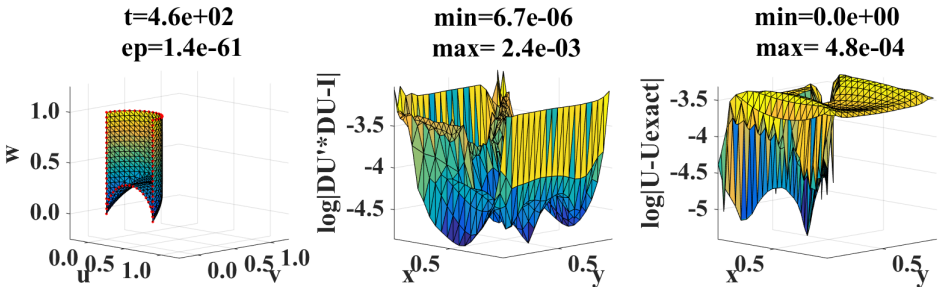


Figure 9: Final shape (left), residuals (middle) and error (right) for Example 4.

the residual values (17) are at most $2.4 \cdot 10^{-3}$ especially in the points where the fold meets the corners. The right plot in Fig. 9 shows the error values (18), which are at most $4.8 \cdot 10^{-4}$, especially away from the fold.

5 Existence and Convergence of Minimizers

5.1 Existence of Minimizers for Fixed Regularization

The existence of minimizers for the functional J in (3) for fixed $\varepsilon > 0$ will first be established. For this purpose, function spaces must be introduced to make the notion of existence precise. Particular use is made of the Sobolev spaces $H^m(\Omega)$ consisting of functions having weak partial derivatives up to order m which lie in the space $L^2(\Omega)$ of Lebesgue measurable and square integrable functions. Also, $H_0^m(\Omega)$ is roughly the subspace of $H^m(\Omega)$ consisting of functions whose derivatives up to order $m - 1$ vanish on $\partial\Omega$. The norm on $L^2(\Omega)$ is denoted by $\|\cdot\|_{L^2(\Omega)}$. The norm on $H^m(\Omega)$ is denoted by $\|\cdot\|_{H^m(\Omega)}$, including the sum of squares of the $L^2(\Omega)$ norm of weak derivatives up to order m . The seminorm $|\cdot|_{H^m(\Omega)}$ includes the sum of squares of the $L^2(\Omega)$ norm of weak derivatives precisely of order m . See [Adams 75] for further details.

For the vector-valued functions appearing in this work, the corresponding Sobolev spaces are Cartesian products of the usual Sobolev spaces, e.g., $H^2(\Omega)^3 = H^2(\Omega) \times H^2(\Omega) \times H^2(\Omega)$. Thus, the functional J of (3) is defined on $\mathcal{D}_J = \{\mathbf{u} \in H^2(\Omega)^3 : \mathbf{u} \text{ satisfies (2)}\}$.

Theorem 1. *Suppose \mathcal{D}_J is not empty. Then there exists at least one $\mathbf{u}^\varepsilon \in \mathcal{D}_J$ which minimizes J in (3) over the set \mathcal{D}_J .*

Proof. Let $\{\mathbf{u}_k\}_{k=1}^\infty$ be a minimizing sequence for J in (3), i.e.,

$$J(\mathbf{u}_{k+1}) \leq J(\mathbf{u}_k), \quad \lim_{k \rightarrow \infty} J(\mathbf{u}_k) = \inf_{\mathbf{u} \in \mathcal{D}_J} J(\mathbf{u}).$$

Using the decomposition $J(\mathbf{u}) = J_1(\mathbf{u}) + 2\varepsilon J_2(\mathbf{u})$

$$J_1(\mathbf{u}) = \int_{\Omega} \|\nabla \mathbf{u}(\mathbf{x})^\top \nabla \mathbf{u}(\mathbf{x}) - I\|_{\mathbb{F}}^2 d\mathbf{x}, \quad J_2(\Omega) = \int_{\Omega} \|\nabla^2 \mathbf{u}(\mathbf{x})\|_{\mathbb{F}}^2 d\mathbf{x} = |\mathbf{u}|_{H^2(\Omega)}^2$$

it is seen that the sequence $\{\mathbf{u}_k\}_{k=1}^\infty$ is bounded in the seminorm of $H^2(\Omega)^3$,

$$|\mathbf{u}_k|_{H^2(\Omega)^3}^2 = J_2(\mathbf{u}_k) \leq J(\mathbf{u}_k)/(2\varepsilon) \leq J(\mathbf{u}_1)/(2\varepsilon).$$

Setting $\hat{\mathbf{u}}_k = \mathbf{u}_k - \mathbf{u}_1$ it follows that $\hat{\mathbf{u}}_k$ vanishes on $\partial\Omega$ and hence $\hat{\mathbf{u}}_k \in H^2(\Omega)^3 \cap H_0^1(\Omega)^3$. On the set of such functions, the $H_2(\Omega)^3$ norm and seminorm are equivalent [Adams 75], i.e., there exist constants c_1 and c_2 such that

$$c_1 |\mathbf{u}|_{H^2(\Omega)^3} \leq \|\mathbf{u}\|_{H^2(\Omega)^3} \leq c_2 |\mathbf{u}|_{H^2(\Omega)^3}, \quad \forall \mathbf{u} \in H^2(\Omega)^3 \cap H_0^1(\Omega)^3.$$

Thus, the sequence $\{\mathbf{u}_k\}_{k=1}^\infty$ is bounded in the norm of $H^2(\Omega)^3$,

$$\begin{aligned} \|\mathbf{u}_k\|_{H^2(\Omega)^3} &= \|\mathbf{u}_1 + \hat{\mathbf{u}}_k\|_{H^2(\Omega)^3} \leq \|\mathbf{u}_1\|_{H^2(\Omega)^3} + \|\hat{\mathbf{u}}_k\|_{H^2(\Omega)^3} \leq \\ &\|\mathbf{u}_1\|_{H^2(\Omega)^3} + c_2 |\hat{\mathbf{u}}_k|_{H^2(\Omega)^3} = \|\mathbf{u}_1\|_{H^2(\Omega)^3} + c_2 |\mathbf{u}_k - \mathbf{u}_1|_{H^2(\Omega)^3} \leq \\ \|\mathbf{u}_1\|_{H^2(\Omega)^3} + c_2 [|\mathbf{u}_k|_{H^2(\Omega)^3} + |\mathbf{u}_1|_{H^2(\Omega)^3}] &\leq (1+c_2) \|\mathbf{u}_1\|_{H^2(\Omega)^3} + c_2 \sqrt{J(\mathbf{u}_1)/(2\varepsilon)}. \end{aligned}$$

Hence, there is a subsequence, again denoted for convenience by $\{\mathbf{u}_k\}_{k=1}^\infty$, which converges weakly in $H^2(\Omega)^3$ to some $\mathbf{u}^\varepsilon \in H^2(\Omega)^3$ [Adams 75]. Since $H^2(\Omega)^3$ is compactly embedded in $H^1(\Omega)^3$ [Adams 75], there is a subsequence, again denoted for convenience by $\{\mathbf{u}_k\}_{k=1}^\infty$, which converges strongly in the norm of $H^1(\Omega)^3$ to \mathbf{u}^ε . It will be shown that \mathbf{u}^ε is a minimizer,

$$\inf_{\mathbf{u} \in \mathcal{D}_J} J(\mathbf{u}) \leq J(\mathbf{u}^\varepsilon) \leq \lim_{k \rightarrow \infty} J(\mathbf{u}_k) = \inf_{\mathbf{u} \in \mathcal{D}_J} J(\mathbf{u})$$

by showing that J_1 is continuous on $H^1(\Omega)^3$ and that J_2 is weakly lower semi-continuous on $H^2(\Omega)^3$, i.e., $\mathbf{u}_k \rightarrow \mathbf{u}^\varepsilon$ in $H^1(\Omega)^3$ implies $J_1(\mathbf{u}_k) \rightarrow J_1(\mathbf{u}^\varepsilon)$ and $\mathbf{u}_k \rightharpoonup \mathbf{u}^\varepsilon$ in $H^2(\Omega)^3$ implies $J_2(\mathbf{u}^\varepsilon) \leq J_2(\mathbf{u}_k)$. Since J_2 is the same as the seminorm on $H^2(\Omega)^3$, the stated property for J_2 is well known [Adams 75]. To show the continuity of J_1 , a direct calculation for $\check{\mathbf{u}}, \hat{\mathbf{u}} \in H^1(\Omega)^3$ gives

$$\begin{aligned} &\|\nabla \check{\mathbf{u}}^\top \nabla \hat{\mathbf{u}} - I\|_{\mathbb{F}}^2 - \|\nabla \hat{\mathbf{u}}^\top \nabla \hat{\mathbf{u}} - I\|_{\mathbb{F}}^2 \\ &= [(\nabla \check{\mathbf{u}} - \nabla \hat{\mathbf{u}})^\top \nabla \hat{\mathbf{u}} + \nabla \hat{\mathbf{u}}^\top (\nabla \check{\mathbf{u}} - \nabla \hat{\mathbf{u}})] : (\nabla \check{\mathbf{u}}^\top \nabla \check{\mathbf{u}} + \nabla \hat{\mathbf{u}}^\top \nabla \hat{\mathbf{u}} - 2I) \end{aligned}$$

showing that the difference $J_1(\check{\mathbf{u}}) - J_1(\hat{\mathbf{u}})$ can be estimated according to

$$|J_1(\check{\mathbf{u}}) - J_1(\hat{\mathbf{u}})| \leq \|\check{\mathbf{u}} - \hat{\mathbf{u}}\|_{H^1(\Omega)^3} \times (\|\check{\mathbf{u}}\|_{H^1(\Omega)^3} + \|\hat{\mathbf{u}}\|_{H^1(\Omega)^3}) (\|\check{\mathbf{u}}\|_{H^1(\Omega)^3}^2 + \|\hat{\mathbf{u}}\|_{H^1(\Omega)^3}^2 + 6|\Omega|)$$

and the continuity of J_1 on $H^1(\Omega)^3$ follows. \square

5.2 Convergence of Minimizers for Vanishing Regularization

The convergence of minimizers \mathbf{u}^ε for the functional J in (3) as $\varepsilon \rightarrow 0$ will now be established. An approach to relaxing the restrictive assumption that there exists a sufficiently smooth \mathbf{u}^\dagger satisfying (1) and (2) is presented in the next subsection.

Theorem 2. *Suppose there is a $\mathbf{u}^\dagger \in H^2(\Omega)^3$ satisfying (1) and (2). Then the minimizers \mathbf{u}^ε of J in (3) converge weakly in $H^2(\Omega)^3$ as $\varepsilon \rightarrow 0$ to some $\mathbf{u}^* \in H^2(\Omega)^3$ satisfying (1) and (2).*

Proof. Recall the decomposition $J(\mathbf{u}) = J_1(\mathbf{u}) + 2\varepsilon J_2(\mathbf{u})$ from the proof of the previous theorem. Since \mathbf{u}^\dagger satisfies (1) and (2), it follows that $J_1(\mathbf{u}^\dagger) = 0$. Since J is minimized by \mathbf{u}^ε , it follows that

$$J_1(\mathbf{u}^\varepsilon) + 2\varepsilon J_2(\mathbf{u}^\varepsilon) = J(\mathbf{u}^\varepsilon) \leq J(\mathbf{u}^\dagger) = 2\varepsilon J_2(\mathbf{u}^\dagger).$$

Taking $J_2(\mathbf{u}^\varepsilon) \leq J_2(\mathbf{u}^\dagger)$ from this inequality gives

$$|\mathbf{u}^\varepsilon|_{H^2(\Omega)^3}^2 = J_2(\mathbf{u}^\varepsilon) \leq J_2(\mathbf{u}^\dagger) = |\mathbf{u}^\dagger|_{H^2(\Omega)^3}^2.$$

Setting $\hat{\mathbf{u}}^\varepsilon = \mathbf{u}^\varepsilon - \mathbf{u}^\dagger$ it follows that $\hat{\mathbf{u}}^\varepsilon$ vanishes on $\partial\Omega$ and hence $\hat{\mathbf{u}}^\varepsilon \in H^2(\Omega)^3 \cap H_0^1(\Omega)^3$. As indicated in the proof of the previous theorem, the $H_2(\Omega)^3$ norm and seminorm are equivalent on the set of such functions [Adams 75]. Hence, the sequence $\{\mathbf{u}^\varepsilon\}_{\varepsilon>0}$ is bounded in the norm of $H^2(\Omega)^3$,

$$\begin{aligned} \|\mathbf{u}^\varepsilon\|_{H^2(\Omega)^3} &= \|\mathbf{u}^\dagger + \hat{\mathbf{u}}^\varepsilon\|_{H^2(\Omega)^3} \leq \|\mathbf{u}^\dagger\|_{H^2(\Omega)^3} + \|\hat{\mathbf{u}}^\varepsilon\|_{H^2(\Omega)^3} \\ &\leq \|\mathbf{u}^\dagger\|_{H^2(\Omega)^3} + c_2 |\hat{\mathbf{u}}^\varepsilon|_{H^2(\Omega)^3} = \|\mathbf{u}^\dagger\|_{H^2(\Omega)^3} + c_2 |\mathbf{u}^\varepsilon - \mathbf{u}^\dagger|_{H^2(\Omega)^3} \\ &\leq \|\mathbf{u}^\dagger\|_{H^2(\Omega)^3} + c_2 |\mathbf{u}^\varepsilon|_{H^2(\Omega)^3} + c_2 |\mathbf{u}^\dagger|_{H^2(\Omega)^3} \leq (1 + 2c_2) \|\mathbf{u}^\dagger\|_{H^2(\Omega)^3}. \end{aligned}$$

Thus, there is a subsequence, again denoted for convenience by $\{\mathbf{u}^\varepsilon\}_{\varepsilon>0}$, which converges weakly in $H^2(\Omega)^3$ to some $\mathbf{u}^* \in H^2(\Omega)^3$ [Adams 75]. Since $H^2(\Omega)^3$ is compactly embedded in $H^1(\Omega)^3$ [Adams 75], there is a subsequence, again denoted for convenience by $\{\mathbf{u}_k\}_{k=1}^\infty$, which converges strongly in the norm of $H^1(\Omega)^3$ to \mathbf{u}^* . As indicated in the proof of the previous theorem, J_1 is continuous on $H^1(\Omega)^3$ and therefore, taking $J_1(\mathbf{u}^\varepsilon) \leq 2\varepsilon |\mathbf{u}^\dagger|_{H^2(\Omega)^3}$ from the first inequality of the proof,

$$J_1(\mathbf{u}^*) \stackrel{0\leftarrow\varepsilon}{\leq} J_1(\mathbf{u}^\varepsilon) \leq 2\varepsilon |\mathbf{u}^\dagger|_{H^2(\Omega)^3} \stackrel{\varepsilon\rightarrow 0}{\rightarrow} 0.$$

It follows that $J_1(\mathbf{u}^*) = 0$, and hence \mathbf{u}^* satisfies (1). Furthermore, according to the property of trace boundary values [Adams 75], it follows from

$$\|\mathbf{u}^* - \mathbf{u}^\varepsilon\|_{L^2(\partial\Omega)^3} \leq c \|\mathbf{u}^* - \mathbf{u}^\varepsilon\|_{H^1(\Omega)^3} \stackrel{\varepsilon\rightarrow 0}{\rightarrow} 0$$

that \mathbf{u}^* satisfies (2) since every \mathbf{u}^ε does. \square

5.3 Relaxing Regularity Assumptions

The assumption for the convergence theorem that there exists at least one $\mathbf{u}^\dagger \in H^2(\Omega)^3$ satisfying (1) and (2) rules out that \mathbf{u}^\dagger may be irregular enough for the paper to be folded. Nevertheless, computations show that the desired convergence may still be expected. Based upon the success of the Mumford-Shah functional for capturing edges in image processing [Mumford and Shah 89], the authors speculate that incorporating the set Γ of folds directly into the functional, e.g., as follows, may be beneficial for Origami,

$$J(\mathbf{u}, \Gamma) = \int_{\Omega \setminus \Gamma} \|\nabla \mathbf{u}(\mathbf{x})^\top \nabla \mathbf{u}(\mathbf{x}) - I\|_{\mathbb{F}}^2 d\mathbf{x} + 2\varepsilon \int_{\Omega} \|\nabla^2 \mathbf{u}(\mathbf{x})\|_{\mathbb{F}}^2 d\mathbf{x} + \mu |\Gamma|.$$

Here, the first integral is calculated only over the set $\Omega \setminus \Gamma$, and $|\Gamma|$ denotes roughly the total length of all folds. The second integral is calculated over the whole set Ω in order to maintain the continuity of \mathbf{u} as $\varepsilon \rightarrow 0$. Since the coefficients of the second-order operator in (4) become negligibly small near a fold in the computational setting, as can be seen from the residual values (17) in Section 4, the effect of the set Γ is damped in practice. Therefore, it may be that the incorporation of Γ into the functional proposed above is purely of theoretical benefit.

References

- [Adams 75] R.A. Adams. *Sobolev Spaces*. Academic Press, 1975.
- [Ciarlet 02] P.G. Ciarlet. *Finite Element Method for Elliptic Problems*. SIAM, 2002.
- [Dacorogna et al. 10] B. Dacorogna, P. Marcellini, and E. Paolini. “Origami and Partial Differential Equations.” *Notices of the AMS* 57:5 (2010), 598–606.
- [Evans 10] L.C. Evans. *Partial differential equations*. American Mathematical Society, 2010.
- [Geretschläger 09] R. Geretschläger. “Folding Curves.” *Proceedings of 4OSME*.
- [Mumford and Shah 89] D. Mumford and J. Shah. “Optimal Approximations by Piecewise Smooth Functions and Associated Variational Problems.” *Communications on Pure and Applied Mathematics* XLII:5 (1989), 577–685.
- [Showalter 77] R.E. Showalter. *Hilbert Space Methods for Partial Differential Equations*. Pitman, 1977.

Stephen Keeling

Institute of Mathematics and Scientific Computing, University of Graz, Graz, Austria,
e-mail: stephen.keeling@uni-graz.at

Robert Geretschläger

Kepler Bundesrealgymnasium, Graz, Austria, e-mail: robert.geretschlaeger@brgkepler.at